Comparative analysis the dual origins of N_2O byproduct on MnO_x, FeO_x and $MnFeO_x$ sphere catalysts for low-temperature SCR of NO with NH_3

Zhichao Chen [a], Rui-tang Guo [b], Shan Ren [a, *], Lin Chen [a], Xiaodi Li [a], Mingming Wang [a]

[a] *College of Materials Science and Engineering, Chongqing University, Chongqing 400044, China*

[b] *College of Energy and Mechanical Engineering, Shanghai University of Electric Power, Shanghai 200090, China*

* Corresponding author email: shan.ren@cqu.edu.cn(S. Ren)

CONTENTS

S1. EXPERIMENTAL DETAILS

S1.1. Catalyst preparation

The Fe-doped MnO_x catalysts were synthesized through a PEG-assisted co-precipitation method. Firstly, 3.042 g (0.018 mol) $MnSO_4 \cdot H_2O$ (99%, Keshi) and 4.848 g (0.012 mol) $Fe(NO_3)_3 \cdot 9H_2O$ (99%, Sinopharm) commercial powders were dissolved in 30 ml distilled water and stirred for 30 minutes. Then, 1 g PEG 4000 (polyethylene glycol, Macklin) weighed was poured into the mixed solution under vigorously stirring for 1 h. The resulting solution was added dropwise to the 100 ml 1M $(NH_4)_2CO_3$ (30% NH_3 basis, Aladdin) precipitator with stirring, and then was kept at pH=9 for the synthesis. After stirring for 1 h, the mixed solution could be aged for three hours, and furthermore stirred for 18 h. In the next step, the obtained suspension was filtered and rinsed with distilled water to neutral pH, then dried at 120 °C for 10 h and finally calcined at 450 °C for 4 h in air atmosphere in a muffle furnace. The solid product powders were compressed and sieved into granules ranging 40–60 mesh for the following experiment. The synthesized catalyst was labeled as $MnFeO_x$ catalyst, especially the molar ratio of Mn:Fe was fixed at 3:2. Besides, the pure MnO_x and FeO_x catalysts were prepared in the same way to provide possible analysis and comparison in the relevant experiment.

S1.2. Catalyst characterization

X-ray powder diffraction (XRD) analysis was performed with a PANalytical X'Pert Powder diffractometer employing Cu Kα radiation at room temperature. The XRD spectra were collected between a 2θ range of 10–90° with 0.02° interval at a scanning speed of 8°/min.

Scanning Electron Micrograph (SEM) measurement was applied to image the surface morphologies of catalysts on Quattro S at the beam energy of 20 kV. Transmission electron microscopy (TEM) and high-resolution transmission electron microscopy (HR-TEM) images were performed on a transmission electron microscope (Tecnai G2 F20, Thermo Fisher, USA) with an accelerating voltage of 150 kV.

Brunauer-Emmett-Teller (BET) surface areas, average pore diameter and total pore volume of catalysts were measured using Micromeritics 3H-2000PS1 operating with physical adsorption of N_2 at -196 °C. Prior to measurements, the catalysts (100mg) were degassed at 200 °C for 4 h under vacuum.

X-ray photoelectron spectroscopy (XPS) measurements were conducted on Thermo ESCALAB250Xi electron spectrometer using a monochromatic Al Kα radiation. Additionally, the C 1s line at 284.8 eV could be applied to calibrate the obtained binding energies.

Hydrogen temperature-programmed reduction (H_2-TPR) analysis was performed on a AutoChem II TPR/TPD 2920 apparatus associated to TCD signal with a H_2 (10%)-Ar mixture as a reductant. In a typical measurement, 100 mg catalysts were firstly treated through an Ar flow at 300 °C for 1 h to remove the adsorbed gaseous impurities. After cooling down to room temperature, the stream could change the Ar into the H_2-Ar mixture, and the temperature was then heated to 800 °C at a constant rate of 10 °C/min. Ammonia temperature-programmed desorption (NH_3-TPD) analysis was similar to that of H_2-TPR. First of all, the pretreatment of catalysts was in exactly the same way. After that, the 100 mg catalysts were saturated with NH_3-Ar mixture at room temperature (about 30 °C) for 1 h, followed the temperature was heated to 900 °C at a rate of 10 °C/min. All the outlet fumes were monitored by TCD signal.

The *in situ* DRIFTS spectra were recorded on Thermo Nicolet iS50 spectrometer with a scanning number of 64 at an interval of 8 cm^{-1}, and equipped with a reaction cell with ZnSe windows. The specific gas system was as follows: 500 ppm NO, 500 ppm NH$_3$, 5 vol% O$_2$, balance N$_2$ and total flow rate was 100 ml/min. Prior to experiment, the catalysts could be purged at 300 °C for 1 h in N$_2$ atmosphere, and background spectra were collected at the target temperature during the cooling process. For gas (NH$_3$/NO+O$_2$) adsorption-desorption experiments, the catalysts were exposed to the corresponding gas for a suitable time at desired temperature. The collected spectra were able to explore the reaction mechanism at different time and temperature between catalysts and reaction gas. For transient reactions between adsorbed species, a typical operating process, prior to injecting NO+O$_2$/NH$_3$/O$_2$ into reaction system, the catalysts were firstly exposed to NH$_3$/NO+O$_2$/NH$_3$ for 50 minutes then N$_2$ purging for 20 minutes.

S2. SUPPLEMENTAL DATA

S2.1. Mass Transfer calculations for NH$_3$-SCR over different catalysts using PBR reaction model (0.05% NO/0.05% NH$_3$/5% O$_2$) [1, 2]

S2.1.1. Mears Criterion for External Diffusion

If $C_1 = \dfrac{-r_A' \rho_b R n}{k_c C_{Ab}} < 0.15$, then external mass transfer effects could be neglected.

Catalysts	T_m	ρ_b	$X_{m, NO}$	$-r_A'$	C_{Ab}	C_1
MnO$_x$	373.15	788	8.10%	1.130×10^{-6}	2.232×10^{-5}	0.053
MnFeO$_x$	373.15	886	14.6%	2.036×10^{-6}	2.232×10^{-5}	0.109

$-r'_A = reaction\ rate$, molg^{-1} s^{-1}

T_m = the maximum temperatures during NH$_3$-SCR kinetic measurements, K.

$X_{m,\ NO}$ = the NO conversion at maximum temperatures.

n = reaction order = 1

R = catalyst particle radius = 1.35×10^{-4} m

ρ_b = bulk density of catalyst bed, kgm^{-3}

= (1 - ф) (ф = porosity or void fraction of packed bed)

ρ_c = solid catalyst density, kgm^{-3}

C_{Ab} = bulk gas concentration of NO at maximum temperatures, kmolm^{-3}

k_c = mass transfer coefficient ≈ 0.1 m s^{-1} [3]

S2.1.2. Weisz-Prater Criterion for Internal Diffusion

If $C_2 = \dfrac{-r'_{A(obs)}\,\rho_c\,R^2}{D_e\,C_{As}} < 1$, then internal mass transfer effects could be neglected.

Catalysts	T_m	ρ_c	$X_{m,\ NO}$	$-r'A(obs)$	C_{As}	C_2
MnO$_x$	373.15	1563	8.10%	1.130×10^{-6}	2.232×10^{-5}	0.144
MnFeO$_x$	373.15	2200	14.6%	2.036×10^{-6}	2.232×10^{-5}	0.365
FeO$_x$	373.15	2983	0	/	2.232×10^{-5}	/

$-r'_{A(obs)}$ = observed reaction rate ≈ $-r'_A$, molg.$^{-1}$ s^{-1}

R = catalyst particle radius = 1.35×10^{-4} m

ρ_b = bulk density of catalyst bed, kgm^{-3}

$= (1 - \phi)$ (ϕ = porosity or void fraction of packed bed)

ρ_c = solid catalyst density, kgm^{-3}

D_e = effective gas-phase diffusivity $\approx 1.0 \times 10^{-5}$, m^{2}s^{-1} [3]

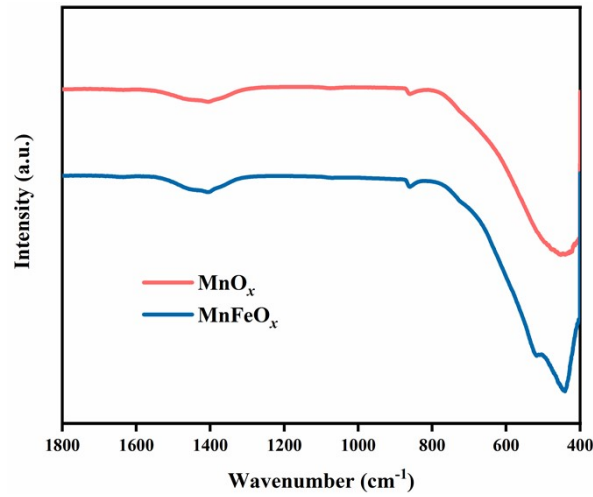C_{As} = gas concentration of NO at the catalyst surface $\approx C_{Ab}$, kmolm^{-3}

Fig. S1. The Infrared spectra of the MnO$_x$ and MnFeO$_x$ catalysts.

Table S1. Surface atom concentration from XPS analysis.

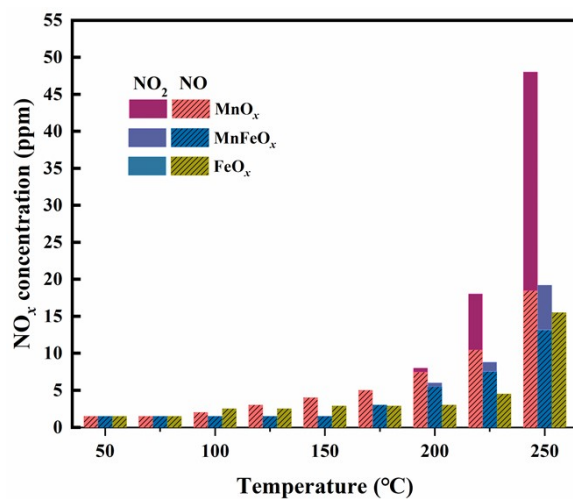| Catalyst	Mn (%)	Fe (%)	O (%)
MnO$_x$	28.7	/	71.3
MnFeO$_x$	19.2	12.3	68.5
FeO$_x$	/	32.1	67.9

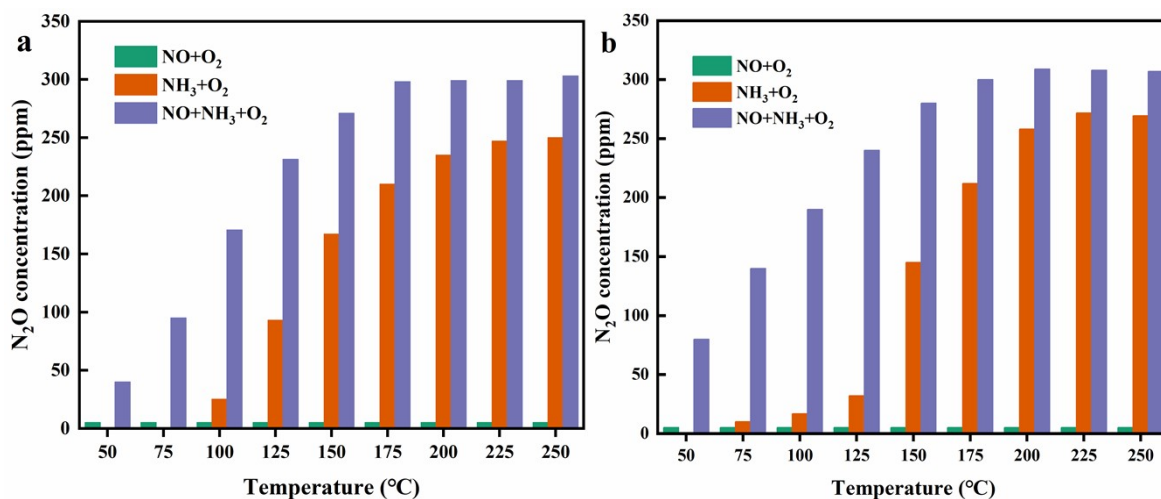**Fig. S2**. NO$_x$ concentration for separate NH$_3$ oxidation process.

Fig. S3. Comparison chart of N$_2$O concentration under different atmosphere with temperature over (a) MnO$_x$ and (b) MnFeO$_x$ catalysts.
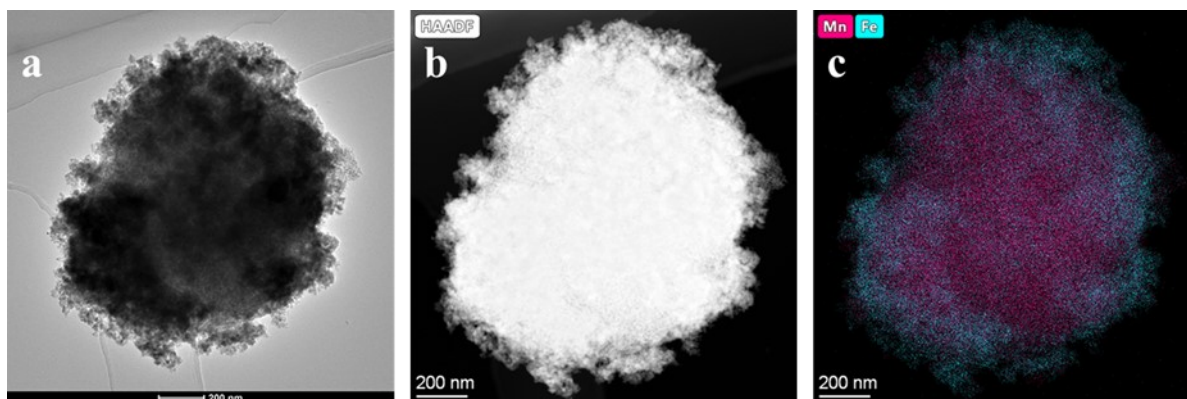
Fig. S4. (a) TEM, (b) HAADF-STEM, and (c) EDS mapping results of MnFeO$_x$ catalyst.

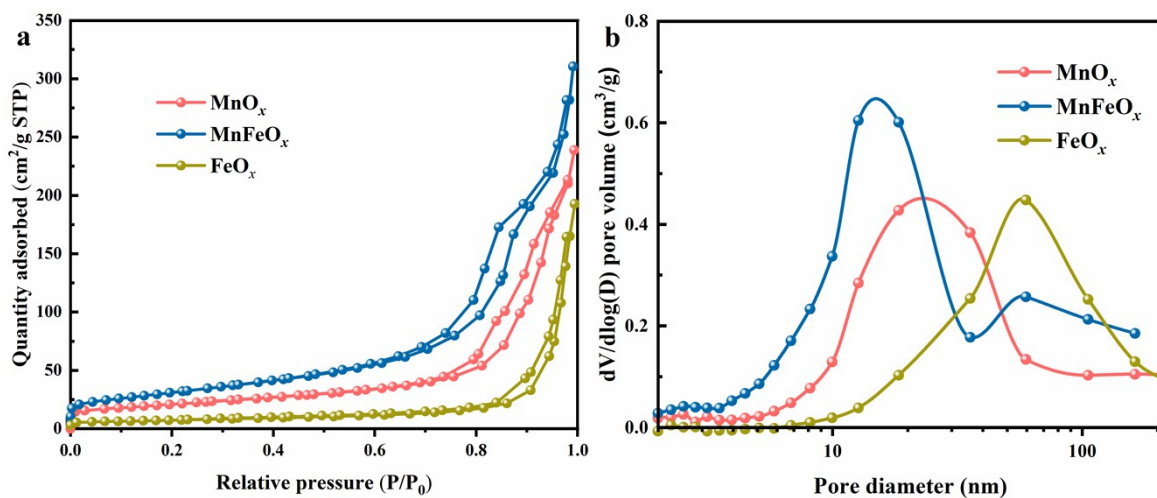**Fig. S5**. (a) Nitrogen adsorption-desorption isotherms and (b) BJH pore diameter distribution curves of MnO$_x$, MnFeO$_x$ and FeO$_x$ catalysts.
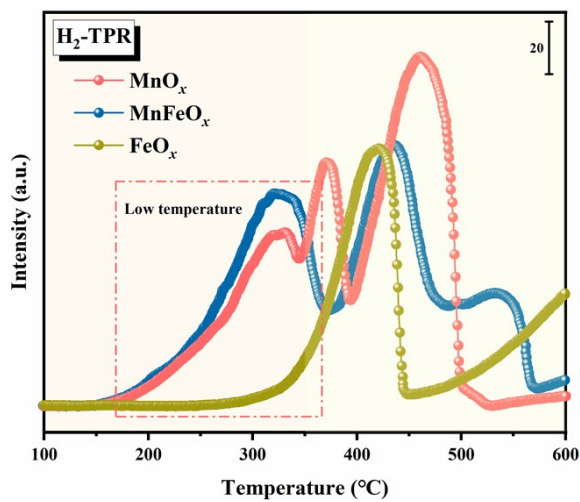

Fig. S6. H$_2$-TPR profiles of MnO$_x$, MnFeO$_x$ and FeO$_x$ catalysts.
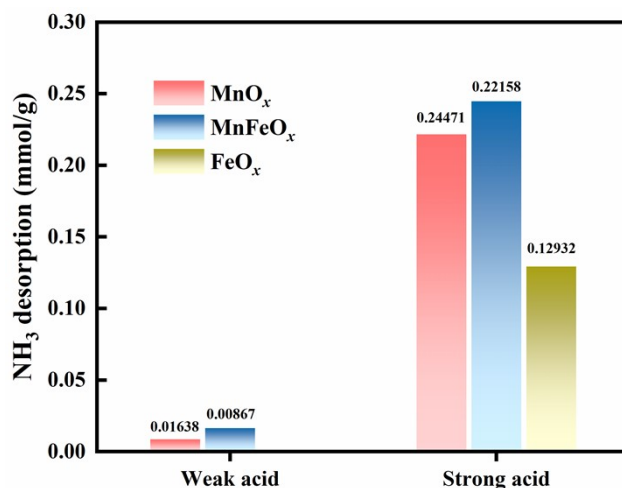
Fig. S7. The amounts of NH_3 desorption on different acid sites over the catalysts.
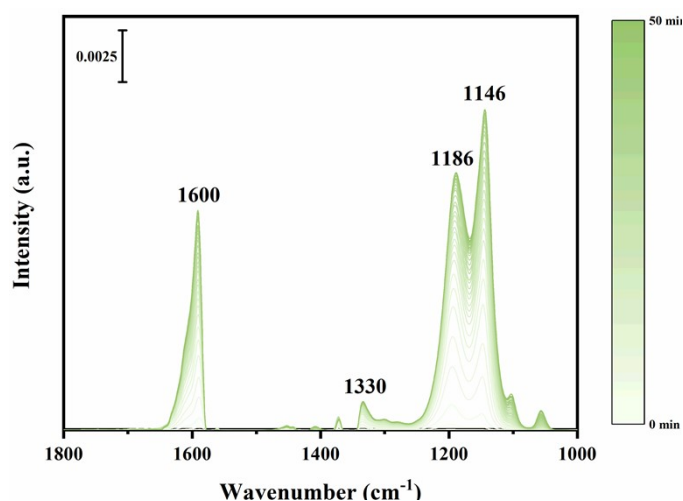
Fig. S8. *In situ* DRIFTS spectra of NH_3 adsorption over FeO_x catalysts at 150 °C

Table S2. Range and assignments of surfaces species obtained during in situ DRIFTS experiments.

Intermediate	Peak position (cm⁻¹)	Exhibited spectra	References
L-NH_3	1152-1185, 1601-1607	Fig. 9; Fig. 10; Fig. 11	[4]
B-NH_4^+	1425	Fig. 9; Fig. 11	[5]
-NH_2/-NH	1560-1570	Fig. 9; Fig. 10; Fig. 11	[5]
Amide (-NH_2) wagging	1341	Fig. 9; Fig. 11	[6]
Oxidation/deformation of	1261	Fig. 11	[7]

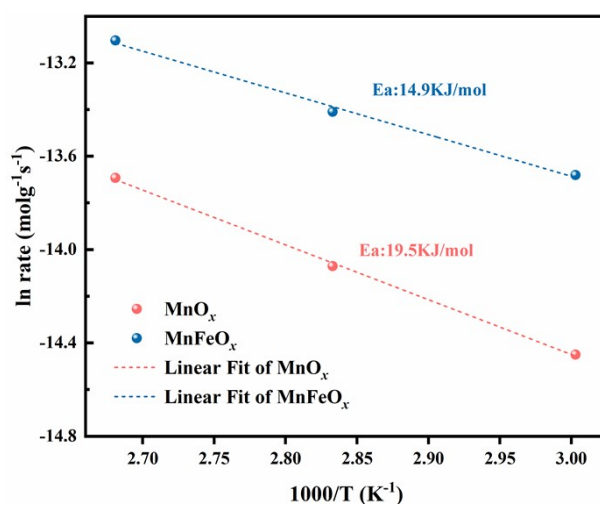| Adsorbed NH₃ species			
NO_3^-	997-1012	Fig. 10; Fig. 12	[7]
Bidentate nitrate (M-O₂NO)	1267	Fig. 10; Fig. 12	[8]
Monodentate nitrate (M-O-NO₂)	1555, 1230	Fig. 10; Fig. 12	[8]
Adsorbed NO₂	1627	Fig. 10; Fig. 12	[9]

Fig. S9. Arrhenius plots of the reaction rates over catalysts. Reaction conditions: 500 ppm [NO], 500 ppm

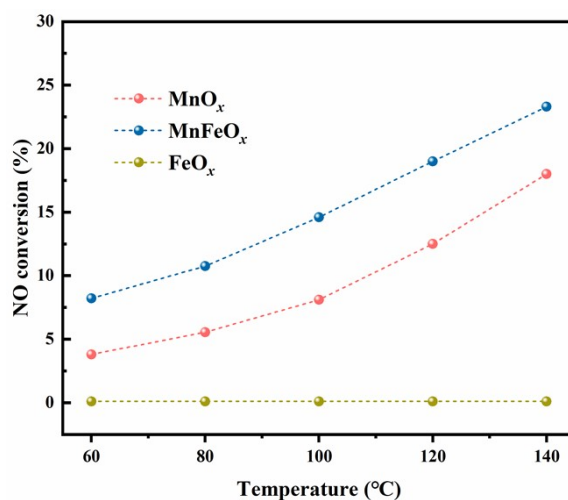[NH₃], 5 vol% [O₂], N₂ balance, MHSV=4500 Lh⁻¹g⁻¹, Tem:150-180 °C.

Fig. S10. NO conversion as a function of temperature in NH₃-SCR reaction at high space velocity over

catalysts. Reaction conditions: [NO] = [NH₃] = 500 ppm, [O₂] = 5 vol.%, N₂ balance, MHSV = 2250 Lg⁻

^{1}h^{-1}.

Table S3. The E_a and TOF (at 100 ^{o}C) values over various catalysts.

Catalysts	E_a (KJ mol^{-1})	TOF $^{@100\ °C}$ (10^{-4}s^{-1})
MnO_x	19.5	14.8
$MnFeO_x$	14.9	16.8
FeO_x	0	0

Table S4. Summary of TOF of various catalysts for NH$_3$-SCR in the previous literatures.

Catalysts	Reaction condition	T (°C)	TOF (10^{-4}s^{-1})
This work	[NO] = [NH$_3$] = 500 ppm, [O$_2$] = 5%, N$_2$ balance, MHSV = 60,000 h^{-1}	100	16.8
MnCeSmTi [10]	[NO] = [NH$_3$] = 0.1%, [O$_2$] = 5%, Ar balance, GHSV = 600,000 h^{-1}	100	8
α-Mn$_2$O$_3$ [11]	[NH$_3$] = [NO] = 500 ppm, [O$_2$] =5%, N$_2$ balance, GHSV = 36,000 h^{-1}.	~100	< 10
Hierc-MnFe$_{0.6}$Co$_{0.4}$O$_x$ [3]	[NH$_3$] = [NO] = 500 ppm, [O$_2$] = 3%, N$_2$ balance, MHSV = 960,000 mLg$_.^{-1}$ h^{-1}	100	5.83
VO$_x$/CeO$_2$ [12]	[NH$_3$] = [NO] = 350 ppm, [O$_2$] = 5%, H$_2$O=4%, GHSV = 399,600 mLg^{-1}h^{-1}	200	10.1

REFERENCES

1. S. Oyama, X. Zhang, J. Lu, Y. Gu and T. Fujitani, *J. Catal.*, 2008, **257**, 1-4.

2.   J. Ji, M. Jing, X. Wang, W. Tan, K. Guo, L. Li, X. Wang, W. Song, L. Cheng, J. Sun, W. Song, C. Tang, J. Liu and L. Dong, *J. Catal.*, 2021, **399**, 212-223.

3.   Y. Li, S. Yang, H. Peng, W. Liu, Y. Mi, Z. Wang, C. Tang, D. Wu and T. An, *J. Catal.*, 2021, **395**, 195-209.

4.   X. Fang, Y. Liu, Y. Cheng and W. Cen, *ACS Catal.*, 2021, **11**, 4125-4135.

5.   Y. Xin, H. Li, N. Zhang, Q. Li, Z. Zhang, X. Cao, P. Hu, L. Zheng and J. A. Anderson, *ACS Catal.*, 2018, **8**, 4937-4949.

6.   M. Jabłońska, A. M. Beale, M. Nocuń and R. Palkovits, *Appl. Catal. B-Environ*, 2018, **232**, 275-287.

7.   C. Gao, B. Xiao, J.-W. Shi, C. He, B. Wang, D. Ma, Y. Cheng and C. Niu, *J. Catal.*, 2019, **380**, 55-67.

8.   Z. Chen, S. Ren, M. Wang, J. Yang, L. Chen, W. Liu, Q. Liu and B. Su, *Fuel*, 2022, **321**, 124113.

9.   W. Chen, S. Yang, H. Liu, F. Huang, Q. Shao, L. Liu, J. Sun, C. Sun, D. Chen and L. Dong, *Environ Sci Technol*, 2022, **56**, 10442-10453.

10.   B. Wang, M. X. Wang, L. N. Han, Y. Q. Hou, W. R. Bao, C. M. Zhang, G. Feng, L. P. Chang, Z. G. Huang and J. C. Wang, *ACS Catal.*, 2020, **10**, 9034-9045.

11.   Z. Fan, Z. Wang, J.-W. Shi, C. Gao, G. Gao, B. Wang, Y. Wang, X. Chen, C. He and C. Niu, *J. Catal.*, 2019, **370**, 30-37.

12.   W. Hu, R. Zou, Y. Dong, S. Zhang, H. Song, S. Liu, C. Zheng, I. Nova, E. Tronconi and X. Gao, *J. Catal.*, 2020, **391**, 145-154.